Journal of the Taiwan Institute of Chemical Engineers 145 (2023) 104816

Contents lists available at ScienceDirect

Journal of the Taiwan Institute of Chemical Engineers

journal homepage: www.journals.elsevier.com/journal-of-the-taiwan-institute-of-chemical-engineers

Partially carbonized wastepaper with excellent mechanical strength for oil-water and emulsion separation

Ming Shi [a], Gang Liu [a], Daning Lang [a], Qianqian Qian [a], Chao Yang [a], Jide Wang [a], Ronglan Wu [a,*], Wei Wang [b,c,*]

[a] Key Laboratory of Oil & Gas Fine Chemicals, School of Chemical Engineering, Xinjiang University, Urumqi 830046, China
[b] Department of Chemistry, University of Bergen, Bergen 5020, Norway
[c] Center for Pharmacy, University of Bergen, Bergen 5020, Norway

ARTICLE INFO

Keywords:
Cellulose
Aerogel
Emulsion separation
Oil/water separation
Wastepaper recycling

ABSTRACT

Background: Taking the treatment of oily sewage and the recycling of wastepaper as the starting point, the idea of using waste to treat waste was used to treat the swage with aerogels made of wastepaper.
Methods: Porous ultralight Fe-functionalized cellulose carbon aerogels (CPFe) were synthesized using wastepaper as raw material through $FeCl_3$ impregnation and low-temperature carbonization.
Findings: CPFe aerogels exhibit excellent physicochemical properties, such as: low density (0.0284 g/cm^3), high porosity (97.32%), and selective absorption capacity for various oil products. The absorption capacity of chloroform reached 62.8 g/g. In addition, it exhibits excellent capacity in emulsion separation for both o/w and w/o types. Droplet size of w/o emulsion reduced by two orders of magnitude. CPFe aerogel is a low-cost, renewable, environmentally friendly material and suitable for large-scale production. It is expected to have broad applications in pollution remediation.

1. Introduction

The discharge of industrial oily wastewater and frequent oil spill accidents have caused a huge waste of oil and water resources and seriously damaged the natural ecosystem [1,2]. In response to global sustainable and green development, the efficient separation and recycling of oil-water mixtures is an important initiative [3,4]. For hydrophobic organic pollutants, it is a better choice to use hydrophobic porous absorption materials [5,6]. Oil absorption performance depends on density and porosity, and more importantly on surface wettability and capillary effect [7]. Among porous materials [8], synthetic aerogel materials such as silicon dioxide [5], carbon nanotubes [9], graphene [10–13] and cellulose [14–17] have attracted attention due to their excellent properties such as ultra-light network structure, high porosity, large specific surface area and strong rigidity [18–21]. However, due to the high price of silica gel, scarce raw materials, difficult synthesis, unique mechanical brittleness, it cannot be used in large-scale oil spill cleaning [22], water environment restoration and other occasions, which is more suitable for fine special physical and chemical environment [23].

In contrast, the preparation of aerogel materials with natural polymer material cellulose has wider research potential [24,25]. Pure cellulose is hydrophilic and cannot be directly used for oil absorption, but after carbonization it can change the surface properties of cellulose to hydrophobic [3]. Carbonized cellulose aerogel can absorb various oils and organic solvents with absorption capacity up to 100 times its own weight, showing good absorption removal of oil pollutants performance [26,27]. At present, various raw materials were used as starting materials for synthesizing cellulose aerogels, such as leaves, wood pulp, cotton, and wheat-straw etc. [28,29] In the process of cellulose extraction, a large number of chemical treatment steps are needed to obtain suitable cellulose, which can be used as waste to a certain extent, but it will also incur other costs [30].

Considering that most of the paper products used in life come from fibers in nature, the use of wastepaper and other rich cellulose derivatives as raw materials will have an added value [31–34]. In this paper, a simple method for preparing iron - based functional cellulose - based carbon aerogel from cellulose extracted from wastepaper was reported. The cellulose extracted from wastepaper was soaked in ferric chloride solution, freeze-dried and carbonized at low temperature to

* Corresponding authors.
E-mail addresses: wuronglan@163.com (R. Wu), wei.wang@uib.no (W. Wang).

https://doi.org/10.1016/j.jtice.2023.104816
Received 26 September 2022; Received in revised form 24 January 2023; Accepted 10 March 2023
Available online 16 March 2023

obtain iron-based functionalized cellulose carbon aerogel (CPFe). The impregnated cellulose aerogel is pyrolyzed at a low temperature (350°C), which is close to the temperature at which maximum mass loss occurs in pure cellulose. In this way, the cellulose material is only partially depolymerized to form carbon fibers on the surface of the aerogel. The resulting carbon fiber is sufficient to change the surface properties of the aerogel, but still retains the elastic skeleton of the cellulose aerogel. In the absorption experiment, CPFe has higher oil absorption capacity and oil absorption rate and is an excellent oil pollutant adsorbent. In addition, CPFe showed good water/oil separation performance for all kinds of emulsions, and the separation effect was significant. This work attempts to demonstrate the value of domestic waste (waste cellulose products) and the resource recovery of waste treatment waste, which provides the direction of higher utilization value for garbage recycling.

2. Experiments and methods

2.1. Materials

Wastepaper was collected from paper recycling bin in our lab, which contained printing paper. Sodium hydroxide (NaOH), sodium hypochlorite (NaClO) and ferric chloride($FeCl_3{\cdot}6H_2O$) were purchased from Tianjin Zhiyuan Chemical Reagent Co., Ltd. Tween 60 and Span 80 were purchased from Tianjin Guangfu Technology Development Co., Ltd. Dimethicone, dimethyl sulfoxide and liquid paraffin were purchased from Shanghai Aladdin Chemical Co., Ltd. Toluene, chloroform and n-hexane were purchased from Tianjin Best Chemical Co., Ltd. Diesel was purchased from China Petroleum & Chemical Corporation. Vacuum pump oil was purchased from Xinjiang Fokker Oil Co., Ltd. Rapeseed oil and soybean oil were purchased from Guangzhou Jinwang Chemical Co., Ltd. Castor oil was purchased from Tianjin Oboke Chemical Co., Ltd. Deionized water was used in all experiments. Diesel oil and soybean oil are industrial grade, and the other reagents are analytical grade.

2.2. Preparation of carbon aerogel

2.2.1. Extraction of cellulose

Wastepaper was chopped into small pieces and briefly washed with water. Then, the wastepaper pieces (4 g) were immersed in 500 mL of NaOH solution (3% wt) with mechanically stirring for 24 h at room temperature. Solid part was separate by filtration and washed with deionized water several times to obtain raw cellulose. Subsequently, the raw cellulose was dispersed into 400 mL NaClO solution (2% wt) and held with stirring at room temperature for 12 h to obtain a white cellulose dispersion. The white cellulose was filtered and washed with water until pH reached 7. The cellulose was dried in a vacuum oven at 80°C for 12 h.

2.2.2. Preparation of cellulose aerogel

The prepared cellulose (2.0 g) was dispersed in 20 mL of 3 mmol/L $FeCl_3$ solution. The dispersion was stirred for 30 minutes and sonicated for 30 minutes. Then, the dispersion was frozen at -20°C for 12 h before freeze-drying for 36 hours at -50°C. After freeze drying, a sponge-like $FeCl_3$-supported cellulose aerogel was yielded. The same method was used to prepare a series of wastepaper cellulose aerogels. Px is used to denote the sample without $FeCl_3$, and here x is the mass content of wastepaper cellulose. For example, P2 means that the wastepaper cellulose is 2% wt. P2Fey is used to denote the samples of $FeCl_3$ loaded P2 aerogels, and here y is 1/10 of the molar concentration of $FeCl_3$ solution.

2.2.3. Preparation of cellulose carbon aerogel

The prepared cellulose aerogel was pyrolyzed in a tube furnace under nitrogen atmosphere. Temperature was increased from 20°C to 350°C at a heating rate of 2°C/min, and kept at 350°C for 120 min. The aerogels underwent dehydration, oxidation, and carbonization to convert cellulose into carbon. After cooling to room temperature, the cellulose carbon aerogel was obtained. The samples are denoted as CPx and CPxFey with the same principle.

2.3. Characterization methods

Morphology of the aerogels were observed by SEM (ZEISS MERLIN Compact Germany). Fourier transform infrared (FTIR) spectra were recorded on VERTEX 70 (Bruker, Germany) using KBr-pallet method. The thermal stability of the samples was measured on a thermogravimetric analyzer SDTQ600 (TA, USA). X-ray diffraction (XRD) was carried out on x-ray diffractometer (Bruker, Germany) in the range of 10-80°. X-ray photoelectron spectra (XPS) were record on a ESCALAB 250Xi (Thermo Fisher Scientific, USA). Al was used as the X-ray target source and the working voltage was 1486.6 eV. The contact angle goniometer (JC2000D4, Shanghai Zhongchen) is used to measure the contact angle at room temperature. The mechanical compressive resistance of aerogel was measured by static mechanics tester (Tinius Oisen, USA), and the compression velocity was 50 mm/min. The particle size of the emulsion was measured by Zetasizer (Nano ZS90, Malvern, UK).

2.4. Density and porosity of aerogel

The mass, diameter, and height of the aerogel before and after carbonization were measured 5 times, and the density (ρ) before and after carbonization of the aerogel is calculated according to

$$\rho = \frac{4m}{\pi d^2 h} \tag{1}$$

where ρ is the aerogel density (g/cm^3), m is the aerogel mass (g), d is the aerogel diameter (cm), and h is the aerogel height (cm).

Calculate the aerogel porosity (P) according to

$$P(\%) = 100 \times \left(1 - \frac{\rho}{\rho_s}\right) \tag{2}$$

where P is the aerogel's porosity (%), and ρ_s is the density of cellulose (g/cm^3).

2.5. Absorption performance

For oil absorption, the weight of the aerogels was measured before the absorption. Afterward, the samples were immersed in different oils or organic solvents until reaching saturation. Then, the surface of the samples was gently wipe with filter paper, followed by quick weighing. Absorption capacity Q (g/g) was calculated by

$$Q = \frac{(m - m_0)}{m_0} \tag{3}$$

where m represents the mass of the aerogel after absorption (g), m_0 is the original mass of the aerogel (g), and Q is the saturated absorption capacity (g/g).

The absorption-desorption cycles were performed for ten times to demonstrate the recycling of the materials.

2.6. Oil-water emulsion separation experiment

Emulsion was prepared by mixing oil and water with volume ratio of 1/10. Tween 60 and Span 80 (1 wt%) were used as emulsifier. The oils used in this experiment included n-hexane, cyclohexane, chloroform, simethicone, and castor oil. For separation of oil in the emulsion, aerogels were added into ten different emulsions. The separation was performed by simply shaking the mixture for approximately 1 minutes. The particle size of the emulsion was measured before and after separation.

3. Results and discussion

3.1. The effect of pyrolysis temperature

Our first question was how pyrolysis temperature would affect the density and porosity of the aerogels? By pyrolyzing the same aerogel at different temperatures, the density and porosity of the products were evaluated, and the results are presented in Fig. 1a. The density of the aerogel decreases significantly with the temperature in the range of 300–350°C. With the further increase of the temperature, the density curve gradually levels off. This result could be explained by the result from TG experiments (see Section 3.2 Fig. 4c). The porosity of the aerogels exhibited a opposite trend. The absorption capacity of the aerogel was also evaluated preliminarily (Fig. 1b). The aerogel pyrolyzed at 350°C showed the highest adsorptive capacity to three types of organic liquids. In addition, cellulose loses most of the weight above 350°C due to the complete carbonization of cellulose. Therefore, without losing the high adsorptive capacity, partially carbonized aerogels of cellulose are maybe a better choice for oil-water and emulsion separation after surface modification.

3.2. Analysis of aerogel morphology and structure

After chemical treatment of wastepaper, we could obtain pure cellulose. Using the cellulose, we synthesized cellulose aerogel and cellulose carbon aerogels. In Fig. 2a and 2b, some cracks appear on the surface of the micron scale cellulose after carbonization, and the surface becomes smoother because the oxygen-containing functional groups on the surface of the cellulose are removed during the pyrolysis process. But the complete form of the cellulose is not affected. No other changes were observed on the surface of the $FeCl_3$ treated cellulose, possibly because $FeCl_3$ was impregnated and attached to the surface of the cellulose in an ionic state (Fig. 2c). After pyrolysis, a layer of ferrite crystals was deposited on the surface of the cellulose. A close-up image of the surface shows that the iron particles have an octahedral shape (Fig. 2d). The elemental state of Fe remains to be further studied by XRD and XPS.

The surface composition of CP2Fe3 was studied by energy dispersive X-ray spectroscopy (EDS). EDS result shows the composition of three main components and their abundance (Fig. 2e). We noticed that the atomic composition of oxygen was 24.27%, which was resulted from cellulose. The oxygen could exist in two sources. One source could be in the frame of the aerogel, meaning the cellulose was not completely pyrolyzed due to the temperature program during the pyrolysis. The other source could be that the oxygen from cellulose react with $FeCl_3$ and forms Fe-O compounds. Therefore, an element mapping was performed on CP2Fe3 sample (Fig. 2f). In the mapping result, the distribution of carbon and oxygen is largely overlapping, strongly indicating that the cellulose is not completely carbonized. However, since Fe is covered on the cellulose backbone, we cannot rule out the possibility of oxygen existing in Fe-O compounds. To fully understand the chemical structure of the products, standard methods of material science were used for the investigation.

To address the bonding chemistry of CP2 and CP2Fe3, we employed XPS and FTIR spectroscopy [34]. Variances between spectra (Fig. 3a) before and after the treatment of $FeCl_3$ reveals significant changes in the properties of peak intensity. In the survey spectra, CP2Fe3 shows two additional peaks (Fe 2p and Cl 2p) [35]. The peak intensity of C 1s significantly reduces in the CP2Fe3 aerogel. A close proximity of Fe binding energy in Fe 2p spectrum (Fig. 3b) reveals two peaks (~724.9 eV and ~711.3 eV), and the binding energy difference (ΔBE) of the two peaks is 13.6 eV. The deconvoluted Fe 2p spectrum showed complex binding information with satellite peaks appearing at 715 eV, 718 eV, 727 eV, and 730 eV. The binding energy of Fe 2p3/2 (~711.3 eV) strongly suggest that Fe is in trivalent state, meaning Fe(III) in $FeCl_3$ maybe remained its valence during pyrolysis [36,37].

The deconvolution of C 1s spectrum shows the binding energies of C-C bond (~284 eV), C-O bond (~286 eV), and C=O bond (~289 eV) (Fig. 3c). The relative intensity of C-C bond binding energy in C 1s spectrum decreased significantly after the treatment of $FeCl_3$. The deconvolution of O 1s spectrum provides valuable information about compounds formed during pyrolysis. The deconvolution of O 1s reveals two binding energies (~531.6 and ~533.6 eV) in CP2. These two binding energies remained in CP2Fe3. Only the intensity of the two binding energies changed. In addition, one more bond formed in CP2Fe3 sample, which gave the binding energy ~530.1 eV. This new bond appeared after the addition of $FeCl_3$, which may suggest a Fe-O bond formed during pyrolysis.

The bond information of the samples was further studied by using FTIR (Fig. 4a). For both P2 and P2Fe3, we still observe the absorption band at 3328 cm^{-1} from OH groups in cellulose. Other characteristic peaks, such as: 2890 cm^{-1} (C–H stretch), 1427 cm^{-1} (C–H bending), 1314 cm^{-1} (C-O stretching), 1158 cm^{-1} (C-O-C stretching), and 1025 cm^{-1} (C-O bending) are marked in the Fig. 4a. After pyrolysis, CP2 and CP2Fe3 still shows weak OH absorption band, indicating that cellulose is partially carbonized. The peak of carbon aerogel at 1636 cm^{-1} (C=O stretching) is stronger than that of cellulose aerogel. There is a weak peak at 1000 cm^{-1} of P2Fe3, which is the Fe-O absorption peak formed after impregnation. In the spectrum of CP2Fe3 after carbonization, there is a weak Fe-O absorption peak at 700 cm^{-1}. After carbonization, the surface of the aerogel changes, and the corresponding position of the Fe-O peak also changes.

The structure of the as-prepared samples was characterized by XRD (Fig. 4b). The aerogels showed X-ray diffraction characteristics of cellulose (2θ=16.9° and 22.7°) crystal structure. After $FeCl_3$ was added into

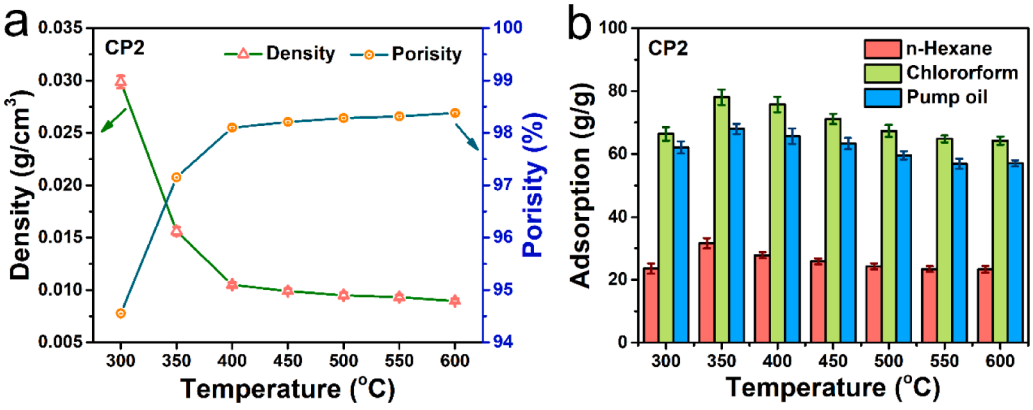

Fig. 1. **(a)** Density and porosity of aerogel CP2 at different pyrolysis temperatures; (**b**) absorption capacity for n-hexane, pump oil and chloroform by using CP2 pyrolyzed at different temperatures.

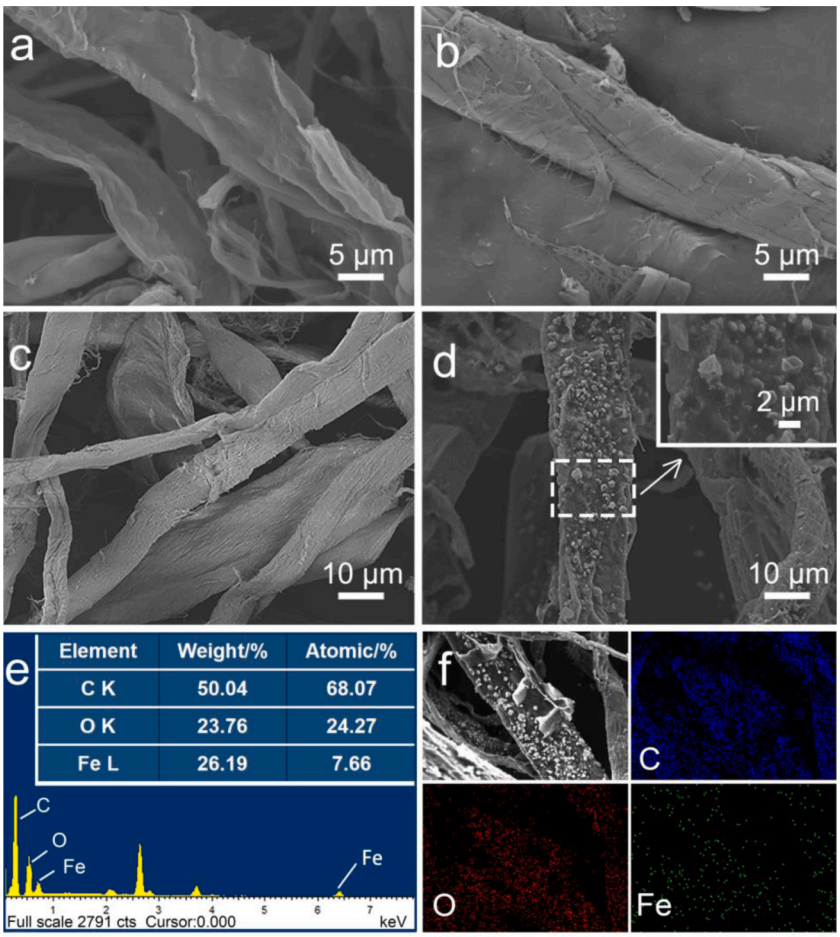

Fig. 2. The SEM images of (**a**) P2, (**b**) CP2, (**c**)P2Fe3, (**d**) CP2Fe3; (**e**) EDS spectrum and elemental content of CP2Fe3; (**f**) element mapping of CP2Fe3.

the aerogel for carbonization, weak crystal structure of cellulose appeared in the XRD pattern. Compared with standard card, it was found that there were multiple peaks of iron compounds, which may be because cellulose and $FeCl_3$ had a variety of chemical reactions in the process of carbonization to produce more forms of iron compounds.

In order to understand the changes in the composition of aerogel during carbonization and the rationality of carbonization conditions, thermal analysis of aerogel and iron source was carried out (Fig. 4c, 4d). The weight loss of P2 mainly occurs in the range of 300 ~ 390°C, and reaches its peak at 355°C. In this temperature range, cellulose loses the oxygen-hydrogen groups on the surface, completes dehydration, and leaves the carbon skeleton. This result is consistent with the results of other studies on the thermal decomposition of cellulose [20]. The carbonized CP2 begins to lose weight at 400°C, and its thermal stability is significantly improved. The thermal decomposition curve of aerogel with $FeCl_3$ added has obvious changes, and the thermal decomposition curve of P2Fe3 has multiple variation ranges, which is due to the addition of a certain amount of $FeCl_3$. Combined with the weightlessness curve of $FeCl_3{\cdot}6H_2O$, it can be found that this phenomenon is consistent with each other. Here we can also find that the decomposition curves of CP2Fe3 and CP2 have a similar trend, and the difference in the residual quantity lies in whether iron source is added. The weight loss of CP2Fe3 is the maximum at 285°C, and the weight loss is basically complete at 420°C. Combined with the decomposition temperature of P2 and the principle of experimental control variables, it is reasonable to set the carbonization temperature of aerogel at 350°C and the holding time at 2h in this experiment. The pyrolysis temperature (350°C) was within the decomposition temperature range of P2 and P2Fe3, which could carbonize most of the cellulose in the aerogel to obtain cellulose skeleton structure. CP2 and CP2Fe3 obtained by decomposition of P2 and P2Fe3 at 350°C have good porosity and mechanical properties due to the large amount of cellulose skeleton structure retained in CP2 and CP2Fe3.

3.3. *Aerogel density, porosity and mechanical properties*

The density and porosity of aerogels are two crucial factor that affects the properties, such as: diffusion and absorption. From the embedded figure, it can be clearly seen that the volume shrinkage of the two aerogels after carbonization. Consequently, and the decrease of density and increase of porosity of the two aerogels can be reflected from the data changes (Fig. 5a, 5b). Since the aerogels are only partially carbonized, which leaves the skeleton of the aerogels unchanged, with the cellulose on the surface carbonized, the porous structure extended after carbonization, leading to an increase of porosity and a decrease of density. With the increased of cellulose content, the density of the aerogels increased, and the porosity decreased (Fig. 5a). With the constant concentration of cellulose, the increase of Fe ions in the aerogels led to the same trend (Fig. 5b).

Mechanical properties of the carbonized aerogels were evaluated with and without the addition of $FeCl_3$ in compressing-recovering cycles (Fig. 6). The trend in the results is obvious. With the increase of cellulose content in the aerogels, the mechanical strength increases. The compressive resistance reached the maximum at the 95% of deformation. The recovering curves do not overlap with the compressing curves for CP aerogels (Fig. 6a), indicating hysteresis during one cycle. The insert image showed one cycle of compressing and recovering for CP2. The volume of CP2 aerogel was compressed to about a quarter of the original volume under external force. After the external force is

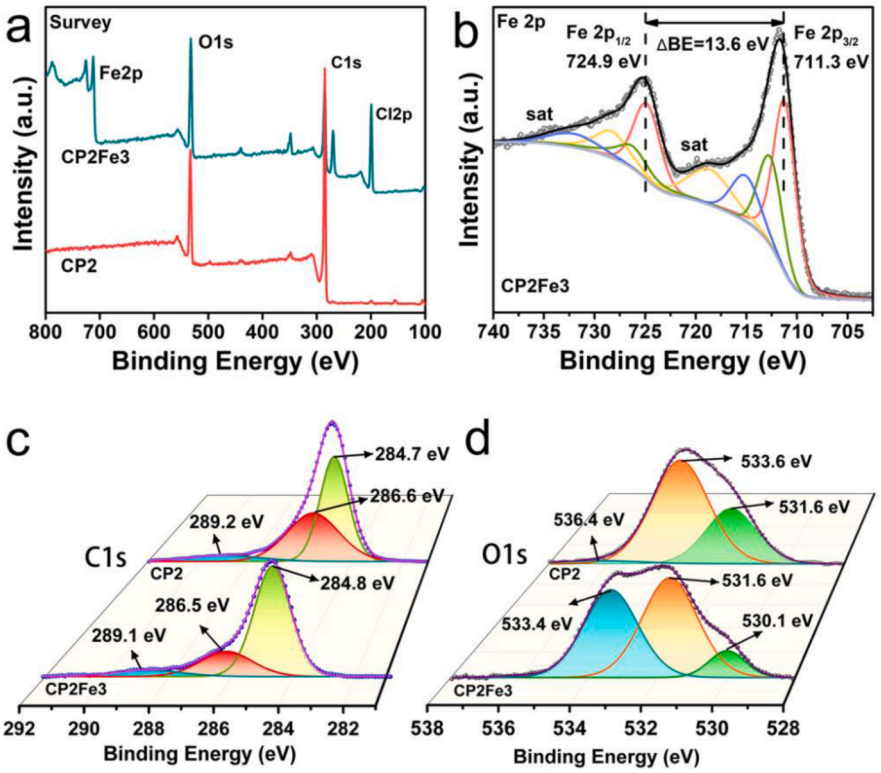

Fig. 3. (**a**) XPS survey spectra of CP2 and CP2Fe3, (**b**) Fe 2p spectrum of CP2Fe3, (**c**) C1s spectrum of CP2 and CP2Fe3, (**d**) O1s spectrum of CP2 and CP2Fe3.

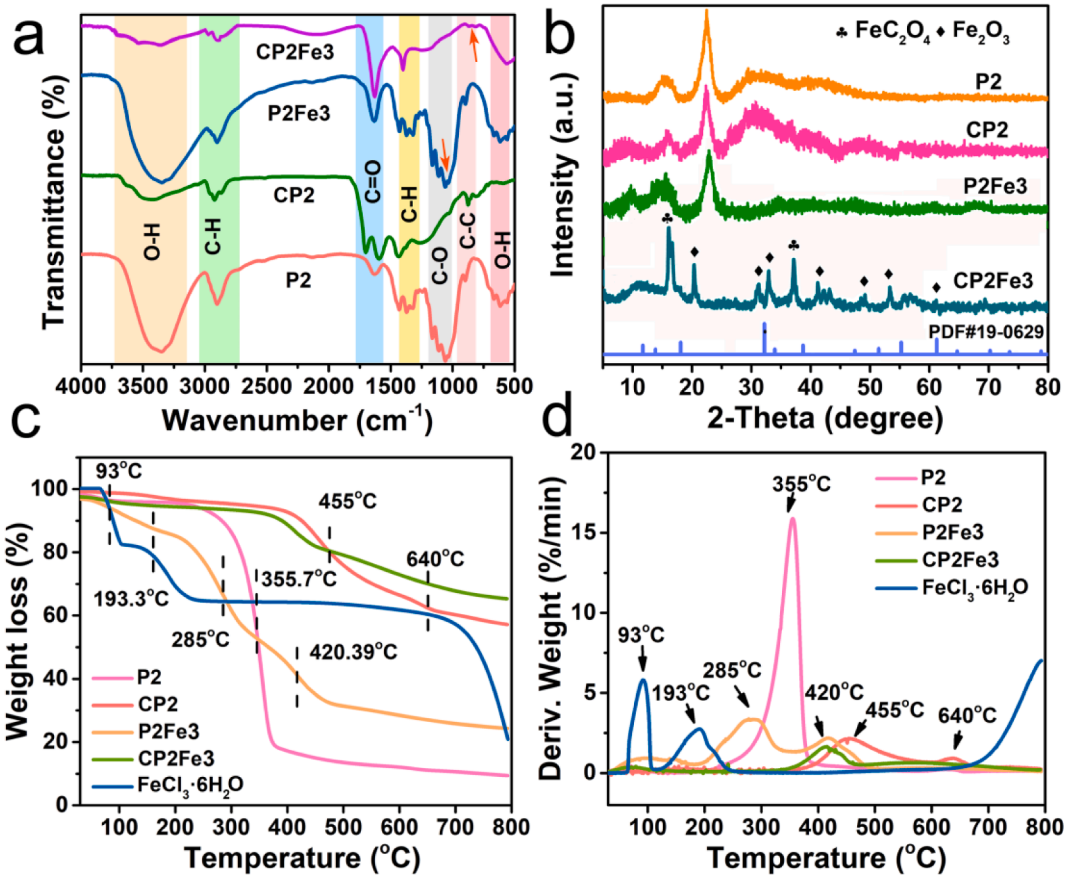

Fig. 4. (**a**) FTIR spectra, (**b**) XRD patterns, (**c**) TG graphs and (**d**) DTG graphs of P2, CP2, P2Fe3 and CP2Fe3.

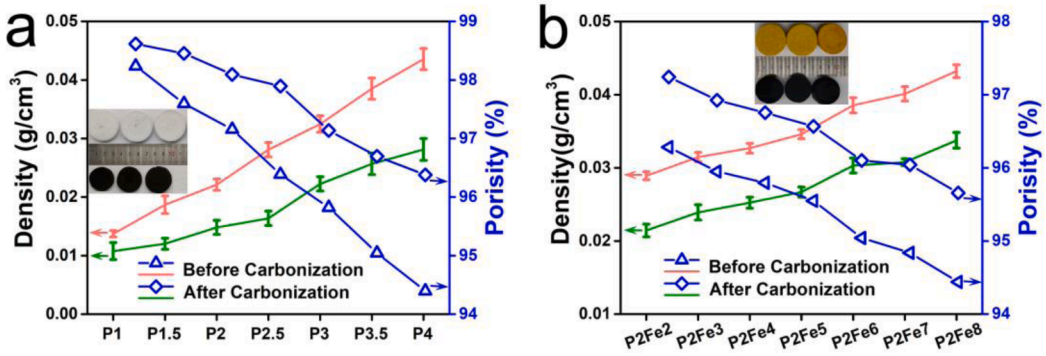

Fig. 5. Density and porosity of (**a**) CP aerogels and (**b**) CP2Fe aerogels.

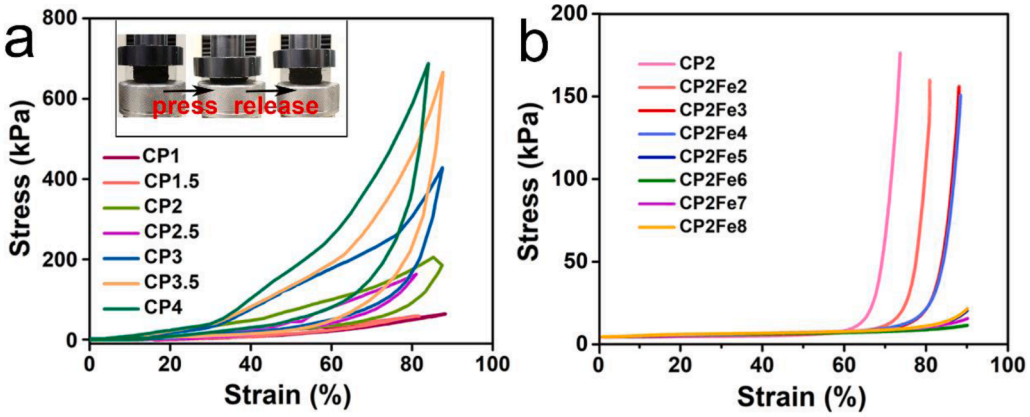

Fig. 6. The mechanical properties of CP aerogels and CPFe aerogels. (**a**) The stress-strain curves of CP aerogels; (**b**) The stress-stain curves of CPFe aerogels.

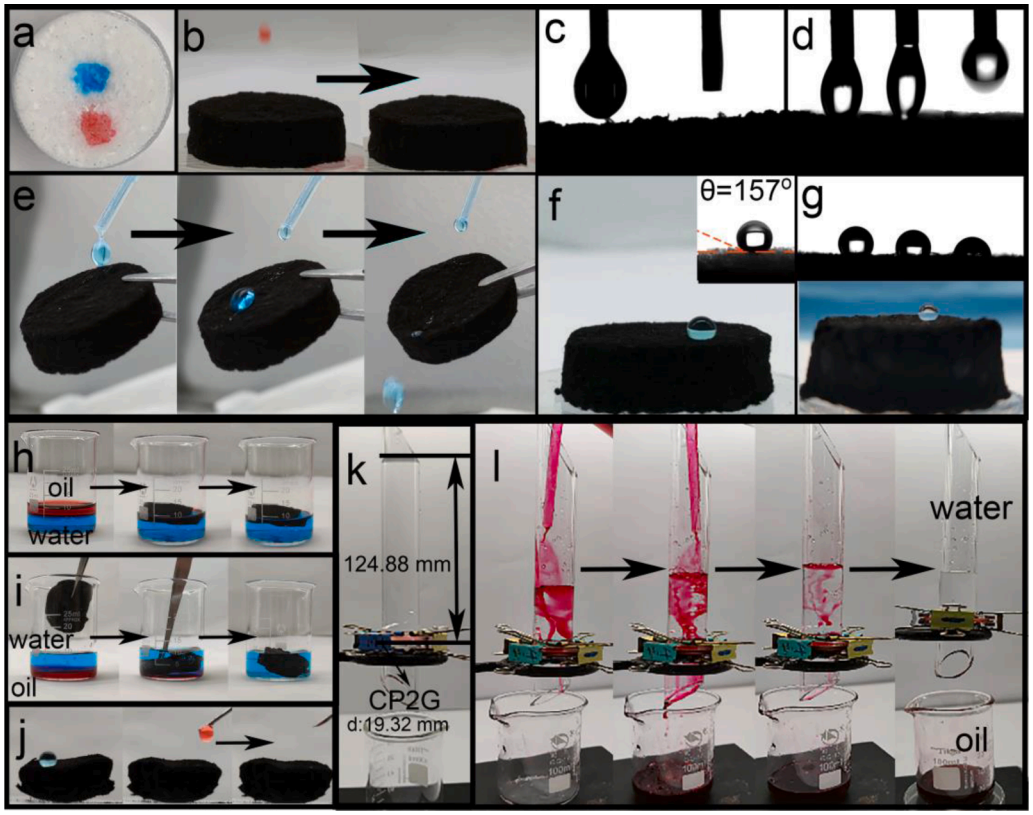

Fig. 7. (**a**) P2 adsorbs oil (colored by red) and water (colored by blue dye); (**b**) oil absorption of CP2; (**c**) oil quickly adsorbed upon touching the surface of CP2; (**d**) demonstration of hydrophobicity of CP2; (**e**) demonstration of water sliding on the surface of CP2; (**f**) contact angle of water on CP2; (**g**) contact angle of water on CP2Fe3, (**h**) soybean oil absorption by CP2 with water in presence; (**i**) chloroform absorption by CP2 with water in presence, (**j**) CP2 surface remains hydrophobic and lipophilic after absorption of oil; (**k**) CP2 subjected to separation column with water on the top, (**l**) demonstration of oil-water separation by CP2.

removed, the aerogel was restored to its original shape, indicating good porosity of the aerogel.

After the addition of $FeCl_3$ in the synthetic procedure, the compressibility of CPFe aerogels actually weakened (Fig. 6b). The more Fe loaded, the weaker the compression resistance was. With high Fe contents, the compressing stress for CPFe aerogels is exceedingly low, even at high strain values. Very interestingly, for the CPFe aerogels with low Fe content, the compressing curves clearly show two stages. At low strain, no stress is detected. The onset of stress was sensed after the strain was over 60%. The curves showed an abrupt increase after the onset. These results indicated that there are clearly two types of frameworks in the aerogel. One of them has low mechanical strength (soft), and the other, on the other hand, is very stiff. Based on the composition of the aerogel, a reasonable assumption can be made that the surface of the aerogel with $FeCl_3$ added is loaded with metal particles after carbonization. During the compression test, the carbon fiber is subjected to the force of metal particles and partial fracture occurs. However, when the compression reaches a certain degree, the carbon fiber of the aerogel can no longer be compressed, so two different curves can be shown in the figure.

3.4. Surface wettability

The wettability of the material is important for the selective separation of oil/water mixtures. The special wettability of cellulose aerogels and cellulose carbon aerogels were evaluated by using a contact angle goniometer (Fig. 7). For P2 aerogel directly obtained from wastepaper, the surface was completely wetted by water and oil, leaving blue water and red oil marks (Fig. 7a), which indicates that the P2 aerogel was amphiphilic with no wetting selectivity.

CP2, however, showed hydrophobic property. Oil drops were absorbed immediately upon touching the surfaces (Fig. 7b and 7d). Water drops slide over after falling on the surface of CP2 aerogel (Fig. 7c and 7e). The static contact angle of CP2 was 157° (Fig. 7f). Fig. 7g shows a water droplet on the surface of CP2. There results of CP2 indicated excellent lipophilic and hydrophobic properties of the aerogel, providing a good foundation for the absorption of oil. CPFe aerogel exhibits hydrophobic response after contact with water droplets, but the hydrophobic property was weakening as time went on. The sharp edges and corners of Fe-O particles loaded on the cellulose carbon skeleton can penetrate the water droplets, reducing the surface tension of the water droplets and slowly spreading on the surface and inside of the composite cellulose carbon aerogel. This phenomenon can be applied to the separation of emulsion. After CPFe reduces the surface tension, the wetting sequence of water and oil on the CPFe surface can form a velocity difference to separate the emulsion.

3.5. Oil-water separation by CP

After the contact angle measurements, separation of the oil-water mixture was performed. The cellulose carbon aerogel was placed in the mixture of hexane/water (Fig. 7h) and in the mixture of chloroform/water (Fig. 7i). The carbon aerogel is hydrophobic and has a low density. CP2 aerogel can quickly absorb n-hexane floating on the water surface. Using tweezers to put it under the water layer, CP2 aerogel can quickly and completely absorb the chloroform layer, and then float on the water surface again. This provides a new strategy for the treatment of the removal of oil spills under the sea. The absorbed oil can be squeezed out from the aerogel. After the absorption, the used aerogel was subjected to contact angle measurement again (Fig. 7j). The original lipophilic and hydrophobic properties remained. CP2 aerogel can also be used to filter oil-water mixture, and separate oil from water (Fig. 7k). The CP2 aerogel was placed in an oil-water separators. Water was placed on the aerogel with height of 124.88 mm. Pouring chloroform and water into the separator (Fig. 7l). It was found that chloroform could pass through carbon aerogel quickly, and the oil-water separation process was very fast.

3.6. Absorptive capacity of CP and CPFe

The absorption capacity of CP aerogels and CPFe aerogels were carried out on three oils (Fig. 8a). The absorption capacity of CP aerogel first increased and then decreased with the increase of cellulose content, and the absorption capacity reached the highest at 1.5% and 2%, respectively. The absorption capacity of the former for chloromethane was 88.5 g/g, while the latter for n-hexane and pump oil were 33 g/g and 70g/g, respectively. The oil absorption capacity reflects the absorption performance of aerogel to some extent. As we all know, the size of oil absorption capacity depends on many factors, such as oil molecular weight, density, volatility, viscosity and so on. To evaluate the comprehensive performance of aerogel, mechanical properties and recycling ability should also be taken into account. Therefore, a series of functional iron aerogel CP2Fe3 was prepared by using CP2 as the base material to study the change of iron load. The absorption of CPFe aerogel decreased monotonically with the increase of $FeCl_3$ content. The absorption capacity of CP2Fe2 for chloroform and pump oil was 65 g/g and 50 g/g, respectively, while the absorption capacity for n-hexane was 30 g/g, which was most likely due to the volatility of n-hexane.

Under the condition that the absorption capacity of CP2Fe2 and CP3Fe3 was similar during the test, CP2Fe3 was selected here for the absorption cycle test in order to be consistent with other applications of Fe-functionalized aerogel in the full paper. The reusability of the aerogel in oil absorption was quantified with CP2 and CP2Fe3 (Fig. 8b and 8c). Ten absorption-desorption cycles were performed for both aerogels. The absorption capacity decreases for both aerogels; however, the decrease in absorption capacity is less significant for CP2 than for CP2Fe3. Over 95% of the initial absorption capacity was remained on the 10^{th} cycle for CP2 after simply squeezing out the absorbed oil. For CP2Fe3 aerogel, 90% of its initial absorption capacity remained on the 10^{th} cycle. According to the mechanical properties of aerogel in Section 3.3, the compression properties of aerogel with iron added will have great changes. After extrusion, the carbon fiber inside the aerogel CP2Fe3 will break more under the action of iron-containing metal oxide particles, and the void structure will be damaged more. Therefore, the reuse ability of aerogel CP2 is affected.

Furthermore, the absorption capacity of the two aerogels to other oils was measured (Fig. 9). In Fig. 9, it can be clearly seen that the absorption capacity of CP2 and CP2Fe3 varies with the type of oil. Among them, the absorption capacity of trichloromethane is the highest, the absorption capacity of CP2 is 88 g/g, CP2Fe3 is 59 g/g, the absorption capacity of n-hexane is the lowest, the absorption capacity of CP2 is 35 g/g, CP2Fe3 is 30 g/g. Among them, toluene has the largest difference in absorption capacity. It is speculated that although toluene has a larger molecular weight, it is different due to the influence of its viscosity and volatility, as well as the non-absorption properties of particles on CP2Fe3 surface. In general, the absorption capacity of CP2Fe3 is lower than that of CP2, also because the iron additive in the aerogel does not have the high absorption capacity of part of the carbonized cellulose.

3.7. Emulsion separation

Emulsion separation is a challenging task both scientifically and industrially [38]. To demonstrate the separation effect of CP2 and CP2Fe3 both w/o emulsions and o/w emulsion with different oil phase were prepared. A typical separation cycle is demonstrated in Fig. 10a. Three o/w emulsions with different oil phase were shown in the first step. The physical properties of emulsion are stable and typical milky white liquid. After the CP2Fe3 aerogel was in the lotion for a few minutes, then filtered out from the emulsion, and left a clear and transparent phase. The process was used for all experiment to separate emulsions. It can be seen from the optical micrograph (Fig 10b) that CP2Fe3 exhibited excellent emulsion separation performance.

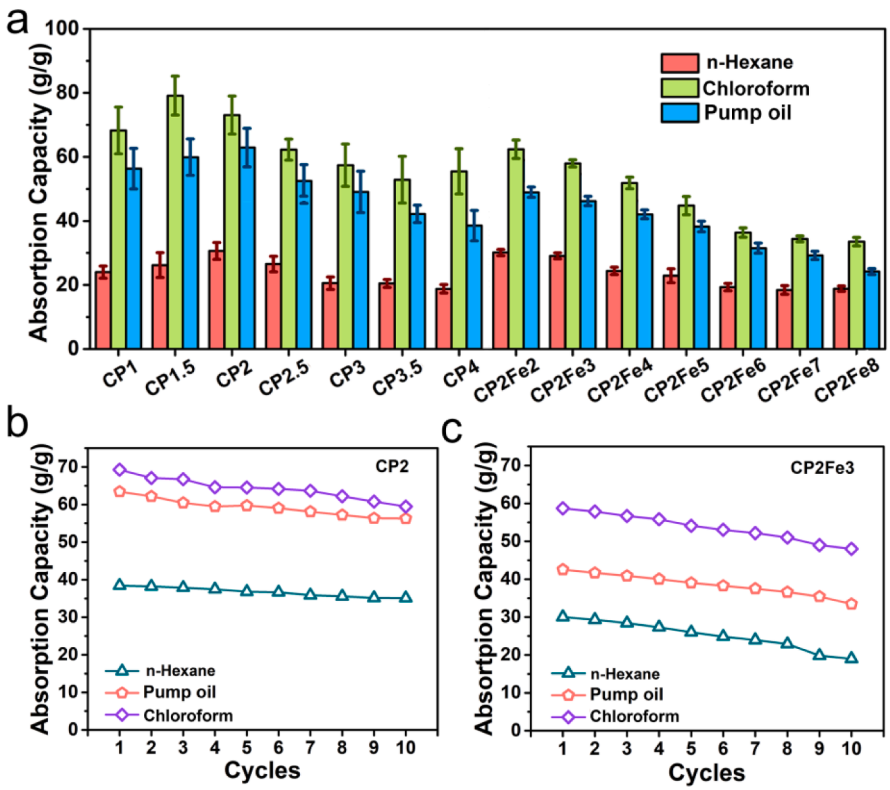

Fig. 8. (**a**) The histogram of the absorption capacity of CPx and CP2Fe for n-hexane, pump oil and chloroform, (**b**) the absorption capacity of CP2 changes in 10 absorption-desorption cycles, (**c**) the absorption capacity of CP2Fe3 changes in 10 absorption-desorption cycles.

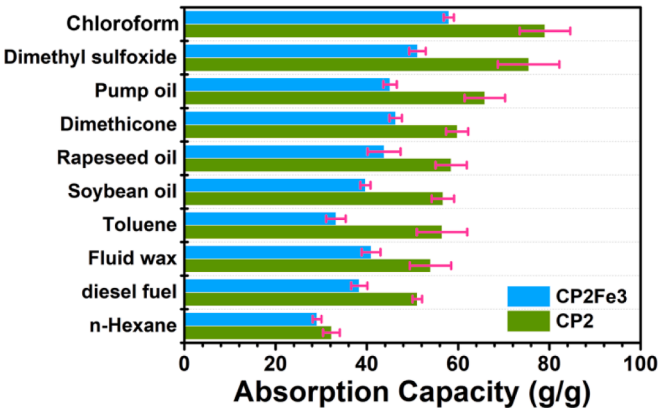

Fig. 9. The absorption capacity of CP2 and CP2Fe3 for other oils.

One of the characteristic changes of the emulsions before and after the separation were the size of the colloidal particles. In Fig. 10c and 10d, the sizes of the colloidal particle were compared by using dynamic light scattering. Five emulsions with different oil phase were used to demonstrate the size change. The initial size of the emulsions is in the range of 1~2 μm. A control experiment was performed for the separation experiments by using Fe_3O_4 particles, which gives slight effects on the size reduction and emulsion separation (Fig. 10c and 10d). On the contrary, CP2 and CP2Fe3 both exhibits excellent properties in removing oil phase in the emulsion. For the w/o emulsions, the particle size reduced to < 100 nm after the separation by CP2, and about 10-20 nm by CP2Fe3 (Fig. 10c). For the o/w emulsions, the same trend was observed (Fig. 10d). For both w/o and o/w emulsions, CP2Fe3 aerogel could completely remove the oil phase. The reminding particles with the size of 10-20 nm should be micelles of Tween 60 and Span 80.

The cyclic performance of CP2 and CP2Fe3 was evaluated for emulsion separation made of chloroform/water system. Due to less effective separation of the o/w emulsion by CP2 aerogel, only size reduction of w/o emulsion was evaluated (Fig 10d). The reuse of the aerogels is simply by squeezing the absorbed oil out of it. Consistent results were reached: CP2 performed less efficient in the emulsion separation than CP2Fe3, and the size reduction became less significant after a few cycles. However, for CP2Fe3, the performance in size reduction was nearly held strong both for the o/w emulsion and the w/o emulsion.

We further studied the reusability of CP2 and CP2Fe3 for separating mixed emulsions. The previously evaluated five w/o emulsions were mixed, and five o/w emulsions were mixed. In Fig. 10e, the cyclic performance of size reduction is presented. Very similar results as shown in Fig. 10d were found. CP2 exhibited a less efficient size-reduction performance comparing to CP2Fe3. For CP2Fe3 aerogels, the size reduction for mixed w/o emulsion is remarkably similar to that for mixed o/w emulsion. The aerogel appeared to be efficient to remove oil phase in also mixed emulsions. The particle size was larger than 20 nm after removing the oil phase, however, the size is larger than the size of pure micelles, therefore, we expect there are still small amount of oil remained in the solution.

Combined with the above content, the separation mechanism of aerogel is simply speculated. In this experiment, although the oil phase of W/O emulsion is continuous phase, the dispersion of the emulsion is relatively strong because the amount of oil phase added in the preparation process is small. For W/O emulsion, CP2 itself has oil hydrophobicity so that CP2 in contact with the emulsion can rely on its special wettability of oil products to absorb the outer layer of the emulsion and leave the internal water phase, the water phase can be mutually condensed to form large droplets. However, the W/O emulsion presents a sticky paste state. In this process, the aerogel cannot adsorb all the oil droplets, so the separation ability of CP2 for W/O emulsion is limited. CP2Fe3 is carbonized to form oleophilic and hydrophobic carbon fiber. At the same time, the surface of the carbon fiber inside the aerogel is

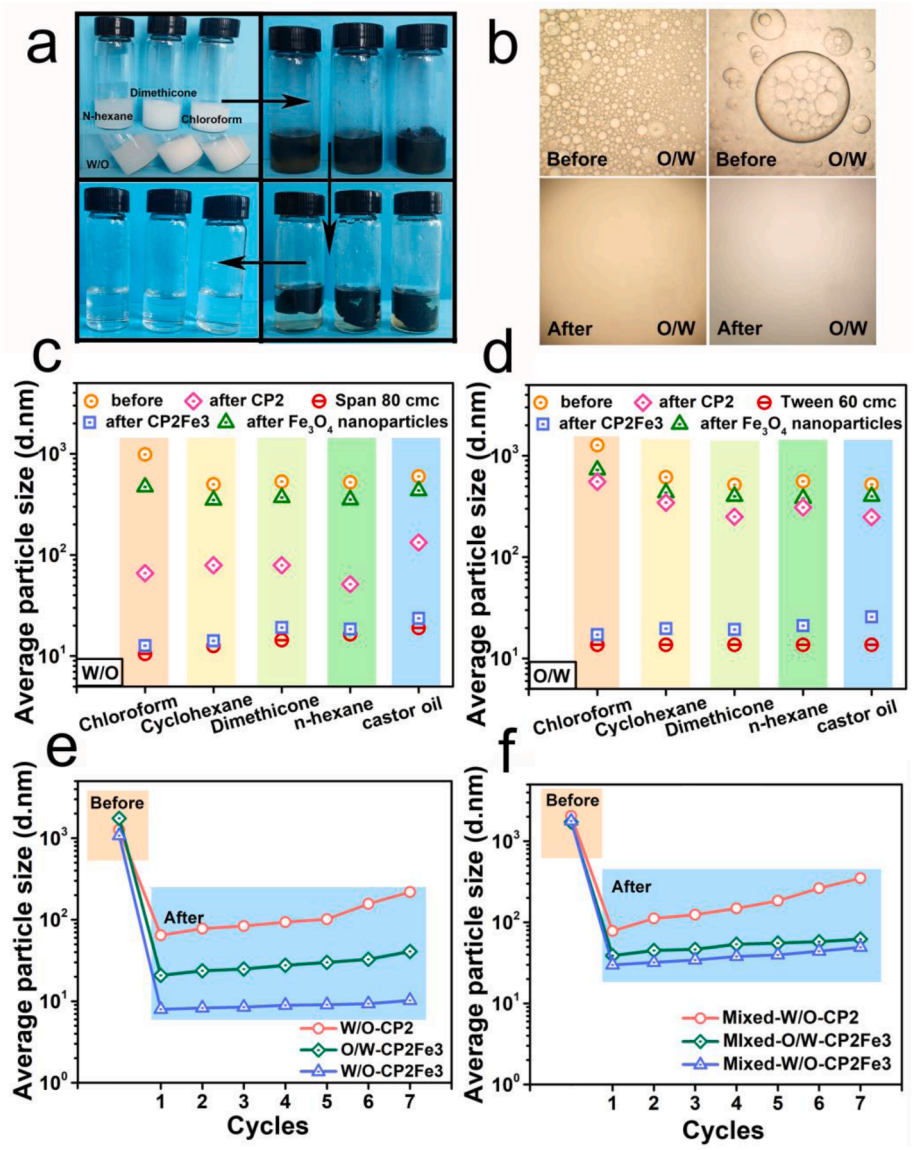

Fig. 10. (**a**) The separation process of three w/o emulsions by CP2Fe3, (**b**) microscope images before and after emulsion separation; (**c**) the size change of five different w/o emulsion before and after the separation process, (**d**) the size change of five different w/o emulsion before and after the separation process, (**e**) the change of particle size in seven cycles of absorption for CP2 in w/o separation and CP2Fe3 in w/o and o/w separation, (**f**) the change of particle size in seven cycles of CP2 in separating mixed w/o emulsion and CP2Fe3 in separating mixed w/o and mixed o/w emulsion.

loaded with Fe-O particles, which can destroy the surface tension of the emulsion and make the emulsion demulsified quickly, so that as many oil droplets can be absorbed by the carbon fiber. The two effects complement each other, so that the aerogel has excellent separation performance for the emulsion. Although CP2Fe3 is oleophilic and hydrophobic, due to the presence of Fe-O particles inside, when the emulsion drops contact CP2Fe3, the sharp Fe-O particles will puncture the stable film on the outer layer of the emulsion drop. The imbalance of the surface tension of the droplet causes the liquid inside the droplet to be exposed to achieve demulsification effect. At this time, the carbon fiber plays different roles on the oil and water. The carbon fiber can quickly absorb the oil droplets flowing out of the droplet, while the excess water phase will gather with each other and pass through the aerogel to achieve emulsion separation.

4. Conclusion

We successfully synthesized CP aerogels and CPFe aerogels with low pyrolysis temperature using wastepaper cellulose as raw material with impregnation of $FeCl_3$. CP aerogels and CPFe aerogels both exhibited lyophilic property, and large porosity (> 95% for both types of aerogels). The adsorption capacity of CP2 for chloroethane and n-hexane was 80 g/g and 35 g/g, and the adsorption capacity of CP2 remained above 95% after ten cycles of adsorption. The adsorption capacity of CP2Fe3 for trichloromethane and n-hexane was 58 g/g and 28 g/g, respectively. After ten cycles, the adsorption capacity was 85% of the initial adsorption capacity. In addition, the demonstration experiment showed that the prepared CP2Fe3 had excellent separation ability for a variety of emulsions. The particle size of the separated emulsion was close to that of the surfactant micelles, and the removal ability remained above 95% after seven cycles of separation.

Declaration of Competing Interest

The authors declare that they have no known competing financial interests or personal relationships that could have appeared to influence the work reported in this paper.

Acknowledgments

This research was financially supported by the Tianshan Youth Program in Xinjiang Province (NO.2020Q011) and the National Natural Science Foundation of China (NO.21868036, NO.32061133005), the Open Project Program of Key Laboratory of Xinjiang Uygur Autonomous

Region (2022D04012). The experimental sample testing and analysis platform was supported by the Ministry Key Laboratory of Oil & Gas Fine Chemicals and the shiyanjia lab (www.shiyanjia.com).

References

[1] Kiliyankil VA, Fugetsu B, Sakata I, Wang ZP, Endo M. Aerogels from copper (II)-cellulose nanofibers and carbon nanotubes as absorbents for the elimination of toxic gases from air. J Colloid Interf Sci 2021;582:950–60.

[2] Cao M, Li SL, Cheng JB, Zhang AN, Wang YZ, Zhao HB. Fully bio-based, low fire-hazard and superelastic aerogel without hazardous cross-linkers for excellent thermal insulation and oil clean-up absorption. J Hazard Mater 2021;403:123977.

[3] Li JJ, Zhou YN, Luo ZH. Polymeric materials with switchable superwettability for controllable oil/water separation: a comprehensive review. Prog Polym Sci 2018; 87:1–33.

[4] Cui JY, Xie AT, Zhou S, Liu SW, Wang QQ, Wu YL, Meng MJ, Lang JH, Zhou ZP, Yan YS. Development of composite membranes with irregular rod-like structure via atom transfer radical polymerization for efficient oil-water emulsion separation. J Colloid Interf Sci 2019;533:278–86.

[5] Cui JY, Zhou ZP, Xie AT, Meng MJ, Cui YH, Liu SW, Lu J, Zhou S, Yan YS, Dong HJ. Bio-inspired fabrication of superhydrophilic nanocomposite membrane based on surface modification of SiO_2 anchored by polydopamine towards effective oil-water emulsions separation. Sep Purif Technol 2019;209:434–42.

[6] Wang Q, Tian D, Hu JG, Huang M, Shen F, Zeng YG, Yang G, Zhang YZ, He JS. Harvesting bacterial cellulose from kitchen waste to prepare superhydrophobic aerogel for recovering waste cooking oil toward a closed-loop biorefinery. ACS Sustain Chem Eng 2020;8:13400–7.

[7] Dilamian M, Noroozi B. Rice straw agri-waste for water pollutant adsorption: relevant mesoporous super hydrophobic cellulose aerogel. Carbohyd Polym 2021; 251:117016.

[8] Yang WJ, Yuen Anthony CY, Li A, Lin B, Chen Timothy BY, Yang W, Lu HD, Yeoh GH. Recent progress in bio-based aerogel absorbents for oil/water separation. Cellulose 2019;26:6449–76.

[9] Juanga RS, Yei YC, Liao CS, Lin KS, Lu HC, Wang SF, Sun AC. Synthesis of magnetic Fe_3O_4/activated carbon nanocomposites with high surface area as recoverable adsorbents. J Taiwan Inst Chem E 2018;000:1–10.

[10] Du XS, Zhou M, Deng S, Du ZL, Cheng X, Wang HB. Poly(ethylene glycol)-grafted nanofibrillated cellulose/graphene hybrid aerogels supported phase change composites with superior energy storage capacity and solar-thermal conversion efficiency. Cellulose 2020;27:4679–90.

[11] Chatterjee S, Ke WT, Liao YC. Elastic nanocellulose/graphene aerogel with excellent shape retention and oil absorption selectivity. J Taiwan Inst Chem E 2020;000:1–9.

[12] Khalilifard M, Javadian S. Magnetic superhydrophobic polyurethane sponge loaded with Fe_3O_4@oleic acid@graphene oxide as high-performance adsorbent oil from water. Chem Eng J 2021;408:127369.

[13] Zhou LJ, Xu ZP. Ultralight, highly compressible, hydrophobic and anisotropic lamellar carbon aerogels from graphene/polyvinyl alcohol/cellulose nanofiber aerogel as oil removing absorbents. J Hazard Mater 2020;388:121804.

[14] Gong ZQ, Yang N, Chen ZX, Jiang B, Sun YL, Yang XD, Zhang LH. Fabrication of meshes with inverse wettability based on the TiO_2 nanowires for continuous oil/water separation. Chem Eng J 2020;380:122524.

[15] Hasan MJ, Petrie FA, Johnson AE, Peltan J, Gannon M, Busch RT, Leontsev SO, Vasquez ES, Urena-Benavides EE. Magnetically induced demulsification of water and castor oil dispersions stabilized by Fe_3O_4-coated cellulose nanocrystals. Cellulose 2021;28:4807–23.

[16] Lang DL, Shi M, Xu X, He SX, Yang C, Wang L, Wu RL, Wang W, Wang JD. DMAEMA-grafted cellulose as an imprinted adsorbent for the selective adsorption of 4-nitrophenol. Cellulose 2021;28:6481–98.

[17] Zhang Y, Yin ML, Lin XH, Ren XH, Huang TS, Kim IS. Functional nanocomposite aerogels based on nanocrystalline cellulose for selective oil/water separation and antibacterial applications. Chem Eng J 2019;371:306–13.

[18] Long SS, Feng YC, He FL, He SS, Hong HC, Yang XR, Zheng LL, Liu J, Gan LH, Long MN. An ultralight, supercompressible, superhydrophobic and multifunctional carbon aerogel with a specially designed structure. Carbon 2020;158:137–45.

[19] Li XQ, Zhang J, Ju ZY, Li Y, Xu JL, Xin JY, Lu XM, Zhang SJ. Facile Synthesis of Cellulose/ZnO Aerogel with uniform and tunable nanoparticles based on ionic liquid and polyhydric alcohol. ACS Sustain Chem Eng 2018;6:16248–54.

[20] Long SS, Feng YC, Liu YZ, Zheng LL, Gan LH, Liu J, Zeng XH, Long MN. Renewable and robust biomass carbon aerogel derived from deep eutectic solvents modified cellulose nanofiber under a low carbonization temperature for oil-water separation. Sep Purif Technol 2021;254:117577.

[21] Wang QZ, Qin Y, Xue CL, Yu HR, Li Y. Facile fabrication of bubbles-enhanced flexible bioaerogels for efficient and recyclable oil adsorption. Chem Eng J 2020; 402:126240.

[22] Moreno-Castilla C, Maldonado-Hódar FJ. Carbon aerogels for catalysis applications: an overview. Carbon 2005;43:455–65.

[23] Li FR, Wang ZR, Huang SC, Pan YL, Zhao XZ. Flexible, durable, and unconditioned superoleophobic/superhydrophilic surfaces for controllable transport and oil-water separation. Adv Funct Mater 2018;28:1706867.

[24] Lang DN, Xu X, Wu RL, Wang W, Shi M, Jia K, Chen SF, Wang JD. Cellulosegtetraethylenepentamine dualfunction imprinted polymers selectively and efectively adsorb and remove 4nitrophenol and Cr(VI). Cellulose 2022;29: 3389–406.

[25] Sirajudheen P, Nikitha MR, Karthikeyan P, Meenakshi S. Perceptive removal of toxic AZO dyes from water using magnetic Fe_3O_4 reinforced graphene oxide–carboxymethyl cellulose recyclable composite: Adsorption investigation of parametric studies and their mechanisms. Surf Interfaces 2020;21:100648.

[26] Ye ZR, Huang KB, Xie M, Yu H, Yang F, Gao MQ, Wang RN, Han L, Wu FX. Eco-friendly, cost-effective, and durable guar gum/citric acid complex coating on mesh for oil/water separation. Int J Biol Macromol 2020;153:641–9.

[27] Li ZD, Zhong L, Zhang T, Qiu FX, Yue XJ, Yang DY. Sustainable, flexible, and superhydrophobic functionalized cellulose aerogel for selective and versatile oil/water separation. ACS Sustain Chem Eng 2019;7:9984–94.

[28] Peydayesh M, Vogt J, Chen XL, Zhou JT, Donat F, Bagnani M, Müller CR, Mezzenga R. Amyloid-based carbon aerogels for water purification. Chem Eng J 2022;449:137703.

[29] Liu LM, Pan YL, Jiang KD, Zhao XZ. On-demand oil/water separation enabled by magnetic super-oleophobic/super-hydrophilic surfaces with solvent-responsive wettability transition. Appl Surf Sci 2020;533:147092.

[30] Srasri K, Thongroj M, Chaijiraaree P, Thiangtham S, Manuspiya H, Pisitsak P, Ummartyotin S. Recovery potential of cellulose fiber from newspaper waste: an approach on magnetic cellulose aerogel for dye adsorption material. Int J Biol Macromol 2018;119:662–8.

[31] Liu XH, Tian F, Zhao X, Du RC, Xu SM, Wang YZ. Recycling waste epoxy resin as hydrophobic coating of melamine foam for high-efficiency oil absorption. Appl Surf Sci 2020;529:147151.

[32] Li ZT, Lin B, Jiang LW, Lin EC, Chen J, Zhang SJ, Tang YW, He FA, Li DH. Effective preparation of magnetic superhydrophobic Fe_3O_4/PU sponge for oil-water separation. Appl Surf Sci 2018;427:56–64.

[33] Zhou WH, Jiang C, Duan X, Song JC, Yuan Y, Chen N. Fe_3O_4/carbonized cellulose micro-nano hybrid for high-performance microwave absorber. Carbohyd Polym 2020;245:116531.

[34] Li LX, Hu T, Li A, Zhang JP. Electrically conductive carbon aerogels with high salt-resistance for efficient solar-driven interfacial evaporation. ACS Appl Mater Inter 2020;12:32143–53.

[35] Yamashita T, Hayes P. Analysis of XPS spectra of Fe^{2+} and Fe^{3+} ions in oxide materials. Appl Surf Sci 2008;254:2441–9.

[36] Yamashita T, Hayes P. Erratum to "Analysis of XPS spectra of Fe^{2+} and Fe^{3+} ions in oxide materials". Appl Surf Sci 2008;254:2441–9. Appl Surf Sci 2009; 255:8194.

[37] Grosvenor AP, Kobe BA, Biesinger MC, McIntyre NS. Investigation of multiplet splitting of Fe 2p XPS spectra and bonding in iron compounds. Surf Interface Anal 2004;36:1564–74.

[38] Chen CL, Weng D, Mahmood A, Chen S, Wang JD. Separation mechanism and construction of surfaces with special wettability for oil/water separation. ACS Appl Mater Inter 2019;11:11006–27.